



Nonreciprocal cavity dark-state polariton and quantum statisticsYu You , Zhengmao Jia, Bing Chen, Da Chen, and Yandong Peng ^{*}*Qingdao Key Laboratory of Terahertz Technology, College of Electronic and Information Engineering, Shandong University of Science and Technology, Qingdao 266590, China*

(Received 21 January 2023; accepted 8 May 2023; published 18 May 2023)

Optical nonreciprocity plays an essential role in optical information communication and information processing. Based on electromagnetically induced transparency, a nonreciprocal cavity dark-state polariton (DSP) could be achieved using spin-biased cold atoms. The DSP induces a nonreciprocal window with high transmission and low insertion loss around the cavity resonant frequency. By decreasing the strength of the control field, the contribution of the atom excitation dominates the behavior of the DSP, which exhibits a narrow cavity linewidth and thus a long lifetime of cavity photons in the form of the DSP. Further, we investigate the nonreciprocity for the statistical properties of the system in the single-atom ($N = 1$) and multiatom ($N > 1$) cases. Due to the existence of DSP, the photon statistics leads to totally different profiles for the light propagating in both directions in the two cases. In the single-atom ($N = 1$) case, the light in the form of DSP shows apparent sub-Poissonian distribution simultaneously with relatively high transmission and a narrow bandwidth corresponding to the one-photon excitation due to quantum interference. Such a quasiparticle may provide a platform for novel applications in nonreciprocal quantum devices and quantum simulation.

DOI: [10.1103/PhysRevA.107.053710](https://doi.org/10.1103/PhysRevA.107.053710)**I. INTRODUCTION**

Optical nonreciprocity has recently attracted a lot of research interest and resulted in novel nonreciprocal devices such as optical isolators, routers, and circulators [1–5], as well as building blocks for the construction of quantum networks [6–8]. Schemes for realizing optical nonreciprocal transmission without magnetic fields have been proposed based on the optical nonlinear effect [9–13], cold atomic Bragg lattices [14,15], dynamic modulation of a material's optical properties [16–19], the optomechanical effect [20–29], the thermal motion of atoms [4,5,30–38], spin-momentum locking [39–48], and so on. In recent years, the nonreciprocal quantum statistics have come into view, including nonreciprocal photon blockade [49–51] and nonreciprocity in photon pair correlations [52], which pave the way toward real quantum nonreciprocal devices.

More recently, cavity polaritons using cold atoms have attracted growing attention due to the potential applications in quantum communications and quantum computation [53,54]. Combining cavity photons with excitations of cold atoms, they possess unique advantages that other systems with only atoms or photons may not have. For example, in the field of quantum simulation, the quasiparticles exhibit not only a richer structure for the hybrid light-matter nature of the excitations but also the ability to address individual sites and enable us to probe out-of-equilibrium many-body phenomena [55–57]. As an exciting development, a nonreciprocal cavity polariton was proposed theoretically and realized experimentally [58]. By combining the properties of cavity polaritons

with optical nonreciprocity, the nonreciprocal cavity bright polariton (BP) may open up a new avenue for novel applications in nonreciprocal devices and provide the potential to study topological photonics in many-body physics. However, such a cavity polariton using two-level cold atoms [58] contains a large contribution from the excited atomic states and suffers from decoherence due to large spontaneous emission. Compared to their counterparts, cavity dark-state polaritons (DSPs) are mixtures of cavity photonic and Raman-like matter branches [59] and have been extensively studied in the past few decades [59–65]. Due to the high tunability of photon lifetimes in the cavity and the immunity to the spontaneous emission of the excited state, many applications based on cavity DSPs have been found, such as cavity linewidth narrowing [62,63], quantum storage [64,65], and photon blockade [66,67].

In this paper, we propose a nonreciprocal cavity DSP by combining intracavity electromagnetically induced transparency (EIT) with spin-biased cold atoms. Different from the nonreciprocal cavity BP realized in [58], the nonreciprocal cavity DSP near the cavity resonance here possesses the following noteworthy features: (i) it is decoupled from the excited state and thus immune to the effects of the spontaneous emission of the excited state; (ii) the bandwidth of the polariton is highly tunable by an external control field, which means the lifetimes of photons in the form of the DSP can be manipulated easily. We also investigate the quantum statistics of the system in the single-atom ($N = 1$) and multiatom ($N > 1$) cases. It can be found that in the presence of the nonreciprocal DSP, the photon statistical properties are also nonreciprocal and exhibit different profiles for light from forward and backward directions in both cases. Due to EIT, the statistics for the left-propagating σ_- -polarized light in the

^{*}pengyd@sdust.edu.cn

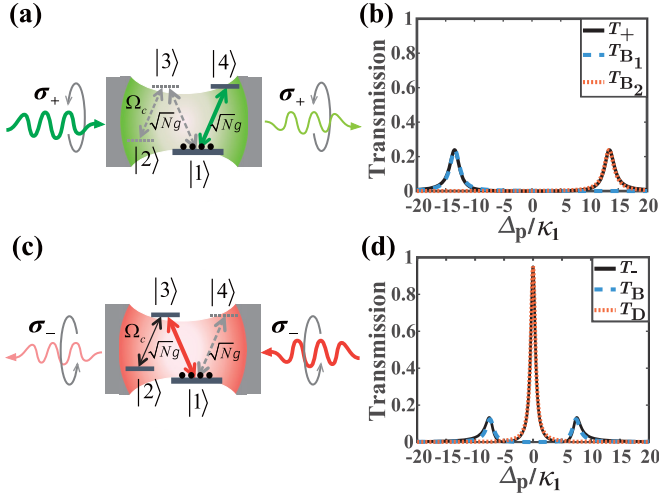


FIG. 1. Schematic illustrations of the nonreciprocal cavity DSP. (a) The σ_+ cavity mode is coupled to the transition $|1\rangle \leftrightarrow |4\rangle$, (b) leading to a vacuum Rabi splitting transmission, with two small side peaks due to the BP states, $|B_1\rangle$ (blue dashed line) and $|B_2\rangle$ (orange dotted line). (c) The σ_- cavity mode couples to the transition $|1\rangle \leftrightarrow |3\rangle$ with an external control field Ω_c driving $|2\rangle \leftrightarrow |3\rangle$, forming a standard Λ -type EIT configuration, and (d) its transmission includes three peaks corresponding to the DSP state $|D\rangle$ and two BP states $|B_\pm\rangle$. The parameters are $Ng_+^2 = 180\kappa_1^2$, $Ng_-^2 = 30\kappa_1^2$, $\Omega_c = 5\kappa_1$, $\Delta_a = \Delta_c = 0$, $\kappa_1 = \kappa_2 = \gamma_3 = \gamma_4$, $\kappa_i = 0.001\kappa_1$, and $\gamma_2 = 0.001\kappa_1$.

form of a DSP can also be manipulated by an external field. In the single-atom case, a DSP performing nonclassical statistics can be obtained by quantum interference between different paths with the proper parameters and has a pronounced sub-Poissonian distribution property and simultaneously possesses high transmission and a narrow bandwidth (i.e., long lifetime of cavity photons) in terms of one-photon excitation. The nonreciprocal DSP proposed here may provide a new platform for nonreciprocal quantum devices and may have the potential for applications in quantum simulation [53–57].

II. THE MODEL SYSTEM

The basic component in our scheme involves an ensemble of N cold atoms trapped in an optical cavity, as illustrated in Fig. 1. The cavity supports degenerate σ_\pm circularly polarized optical modes. We assume that the right-propagating input light field is σ_+ -polarized and excites only the σ_+ -polarized cavity mode and versa vice, which is feasible in the present experiments [46–48,58]. The relevant levels of the atoms include two ground states, $|1\rangle$ and $|2\rangle$, as well as two degenerate excited states, $|3\rangle$ and $|4\rangle$. Each of the atoms is initially prepared in the spin-biased hyperfine ground state $|1\rangle$ with the polarization-dependent transition $|1\rangle \leftrightarrow |4\rangle$ ($|3\rangle$) coupled only to the σ_+ -polarized (σ_- -polarized) cavity mode. An external field with Rabi frequency Ω_c drives the transition between $|2\rangle$ and $|3\rangle$, which can control the σ_- -polarized transition $|1\rangle \leftrightarrow |3\rangle$ through the EIT process.

Under the rotating-wave and electric dipole approximations, the non-Hermitian Hamiltonian \hat{H} of this system, consisting of a cavity with N four-level atoms, can be

written as

$$\begin{aligned} \hat{H} = & \left(\omega_a - \frac{i\kappa}{2} \right) (\hat{a}_+^\dagger \hat{a}_+ + \hat{a}_-^\dagger \hat{a}_-) + \sum_{j=1}^N \sum_{l=1}^4 (\omega_l - i\gamma_l) \hat{\sigma}_{ll}^{(j)} \\ & + \sum_{j=1}^N [g_+^{(j)} \hat{a}_+ \hat{\sigma}_{41}^{(j)} + g_-^{(j)} \hat{a}_- \hat{\sigma}_{31}^{(j)} + \Omega_c \hat{\sigma}_{32}^{(j)} e^{-i\omega_c t} + \text{H.c.}] \\ & + [i\sqrt{\kappa_1} \hat{a}_+^\dagger E_{p+} e^{-i\omega_p t} + i\sqrt{\kappa_2} \hat{a}_-^\dagger E_{p-} e^{-i\omega_p t} + \text{H.c.}]. \quad (1) \end{aligned}$$

Here, \hat{a}_\pm is the annihilation operator of the σ_\pm -polarized cavity mode, and $\hat{\sigma}_{lm}^{(j)} = |l\rangle_j \langle m|$ ($l, m = 1, 2, 3, 4$) are the atomic raising and lowering operators for $l \neq m$ and the atomic population operators for $l = m$. ω_l and γ_l ($l = 1, 2, 3, 4$) are the energy and decay rate of the $|l\rangle$ state, and we set $\gamma_1 \equiv 0$. $g_\pm^{(j)}$ is the coupling strength between the σ_\pm -polarized cavity mode and the j th single atom. ω_a and ω_p are the angular frequencies of the cavity mode and the probe field, respectively. κ_1 (κ_2) is the decay rate of the cavity modes through the left (right) mirror, and the total decay rate of the cavity is $\kappa = \kappa_1 + \kappa_2 + \kappa_i$, with κ_i being the intrinsic cavity decay rate. $E_{p\pm}$ represents the strength of the σ_\pm -polarized input light, which can drive only the σ_\pm cavity mode, respectively.

In the rotating frame defined by the unitary transformation

$$\begin{aligned} \hat{U} = \exp \left\{ -i\omega_p (\hat{a}_+^\dagger \hat{a}_+ + \hat{a}_-^\dagger \hat{a}_-) \right. \\ \left. - i \sum_{j=1}^N \left[\sum_{l=1}^4 \omega_l \hat{\sigma}_{ll}^{(j)} + \omega_p (\hat{\sigma}_{44}^{(j)} + \hat{\sigma}_{33}^{(j)}) \right. \right. \\ \left. \left. + (\omega_p - \omega_c) \hat{\sigma}_{22}^{(j)} \right] t \right\}, \quad (2) \end{aligned}$$

the effective Hamiltonian $\hat{H}' = \hat{U}^\dagger \hat{H} \hat{U} - i\hat{U}^\dagger \frac{\partial \hat{U}}{\partial t}$ ($\hbar \equiv 1$) can be written as

$$\begin{aligned} \hat{H}' = & \left(\Delta_p - \frac{i\kappa}{2} \right) (\hat{a}_+^\dagger \hat{a}_+ + \hat{a}_-^\dagger \hat{a}_-) - \sum_{j=1}^N \sum_{l=1}^4 i\gamma_l \hat{\sigma}_{ll}^{(j)} \\ & + \sum_{j=1}^N [(\Delta_a + \Delta_p) (\hat{\sigma}_{44}^{(j)} + \hat{\sigma}_{33}^{(j)}) \\ & + (\Delta_a + \Delta_p - \Delta_c) \hat{\sigma}_{22}^{(j)}] \\ & + \sum_{j=1}^N [g_+^{(j)} \hat{a}_+ \hat{\sigma}_{41}^{(j)} + g_-^{(j)} \hat{a}_- \hat{\sigma}_{31}^{(j)} + \Omega_c \hat{\sigma}_{32}^{(j)} + \text{H.c.}] \\ & + [i\sqrt{\kappa_1} \hat{a}_+^\dagger E_{p+} + i\sqrt{\kappa_2} \hat{a}_-^\dagger E_{p-} + \text{H.c.}], \quad (3) \end{aligned}$$

in which the detunings are defined as $\Delta_p = \omega_a - \omega_p$, $\Delta_a = \omega_D - \omega_1 - \omega_a$, and $\Delta_c = \omega_D - \omega_2 - \omega_c$. Here, we define $\omega_3, \omega_4 \equiv \omega_D$. In the following, we assume that each atom has the same strength when coupling to the cavity mode and then take $g_+^{(j)} \equiv g_+$ and $g_-^{(j)} \equiv g_-$ ($j = 1, 2, \dots, N$).

III. NONRECIPROCAL CAVITY DARK-STATE POLARITON

When input light is incident from the left side of the cavity [shown in Fig. 1(a)], the σ_+ -polarized cavity mode is excited and is coupled only to the transitions $|1\rangle \leftrightarrow |4\rangle$. The system can be simplified as N cold cavity-trapped two-level atoms [58]. As for the light incident from the right side of the cavity [as shown in Fig. 1(c)], the σ_- -polarized cavity mode is excited and is coupled only to the transitions $|1\rangle \leftrightarrow |3\rangle$, and then a standard Λ -type EIT configuration is formed [68]. In the weak-field approximation, the steady-state solution of the cavity modes \hat{a}_+ and $\hat{\sigma}_{14}^{(j)}$ for the right-propagating input light and \hat{a}_- and $\hat{\sigma}_{12}^{(j)}$ for the left-propagating input light can be derived, respectively, as (see Appendix A for more details)

$$\hat{a}_+ = \frac{\sqrt{\kappa_1} E_{p+}}{i\Delta_p + \frac{\kappa}{2} + \frac{Ng_+^2}{i(\Delta_a + \Delta_p) + \gamma_4}}, \quad (4a)$$

$$\hat{\sigma}_{14}^{(j)} = -\frac{g_+ \hat{a}_+}{\Delta_a + \Delta_p - i\gamma_4}, \quad (4b)$$

$$\hat{a}_- = \frac{\sqrt{\kappa_2} E_{p-}}{i\Delta_p + \frac{\kappa}{2} + \frac{Ng_-^2}{i(\Delta_a + \Delta_p) + \gamma_3 + \frac{\Omega_c^2}{i(\Delta_a + \Delta_p - \Delta_c) + \gamma_2}}}, \quad (4c)$$

$$\hat{\sigma}_{12}^{(j)} = \frac{\Omega_c g_- \hat{a}_-}{(\Delta_a + \Delta_p - i\gamma_3)(\Delta_a + \Delta_p - \Delta_c - i\gamma_2) - \Omega_c^2}. \quad (4d)$$

According to the two-side cavity input-output formulation [69], we have $\hat{a}_{\text{out}+} = \sqrt{\kappa_2} \hat{a}_+$ and $\hat{a}_{\text{out}-} = \sqrt{\kappa_1} \hat{a}_-$.

Further, we define two cavity bright polariton modes for the right-propagating input case: $\hat{B}_1 = \frac{1}{\sqrt{2}}(\hat{a}_+ - \hat{S}_{14})$ and $\hat{B}_2 = \frac{1}{\sqrt{2}}(\hat{a}_+ + \hat{S}_{14})$, with the collective atomic operator $\hat{S}_{14} = \frac{1}{\sqrt{N}} \sum_{j=1}^N |1\rangle_j \langle 4|$ [60]. Then, the transmissions corresponding to the cavity mode \hat{a}_+ and the cavity BP modes \hat{B}_1 and \hat{B}_2 are defined as $T_+ = \frac{\langle \hat{a}_{\text{out}+}^+ \hat{a}_{\text{out}+} \rangle}{|E_{p+}|^2} = \frac{\kappa_2 \langle \hat{a}_+^+ \hat{a}_+ \rangle}{|E_{p+}|^2}$, $T_{B_1} = \frac{\kappa_2 \langle \hat{B}_1^+ \hat{B}_1 \rangle}{2|E_{p+}|^2}$, and $T_{B_2} = \frac{\kappa_2 \langle \hat{B}_2^+ \hat{B}_2 \rangle}{2|E_{p+}|^2}$, respectively. Figure 1(b) shows the transmissions for the cavity mode \hat{a}_+ and the polariton modes \hat{B}_1 and \hat{B}_2 . Due to the interaction between the cavity mode \hat{a}_+ and the transitions $|1\rangle \leftrightarrow |4\rangle$, the vacuum Rabi splitting spectrum appears, and its two small side peaks are at frequencies $\omega_a - \sqrt{Ng_+}$ and $\omega_a + \sqrt{Ng_+}$, which correspond to the BP states $|\hat{B}_1\rangle$ and $|\hat{B}_2\rangle$ when $\Delta_a = \Delta_c = 0$. The two cavity polaritons separate well if the collective coupling strength $\sqrt{Ng_+}$ is relatively large. The nearly resonant input field almost dissipates and cannot be transmitted from the right mirror.

For the left-propagating input case, a cavity BP mode $\hat{B} = \sin\theta \hat{a}_- + \cos\theta \hat{S}_{12}$ and a cavity DSP mode $\hat{D} = \cos\theta \hat{a}_- - \sin\theta \hat{S}_{12}$ are defined with $\cos\theta = \frac{\Omega_c}{\sqrt{Ng_-^2 + \Omega_c^2}}$, $\sin\theta = \frac{\sqrt{Ng_-}}{\sqrt{Ng_-^2 + \Omega_c^2}}$, and the collective atomic operator $\hat{S}_{12} = \frac{1}{\sqrt{N}} \sum_{j=1}^N |1\rangle_j \langle 2|$. The transmissions corresponding to the cavity mode \hat{a}_- , the cavity BP mode \hat{B} , and the cavity DSP mode \hat{D} are given by $T_- = \frac{\langle \hat{a}_{\text{out}-}^+ \hat{a}_{\text{out}-} \rangle}{|E_{p-}|^2} = \frac{\kappa_1 \langle \hat{a}_-^+ \hat{a}_- \rangle}{|E_{p-}|^2}$, $T_B = \frac{\kappa_1 \sin^2\theta \langle \hat{B}^+ \hat{B} \rangle}{|E_{p-}|^2}$, and $T_D = \frac{\kappa_1 \cos^2\theta \langle \hat{D}^+ \hat{D} \rangle}{|E_{p-}|^2}$, respectively. The intracavity EIT in-

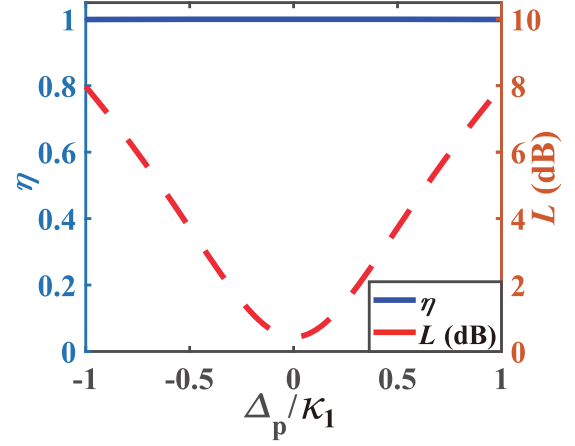


FIG. 2. The contrast ratio η and the insertion loss L versus the normalized frequency detuning Δ_p/κ_1 . Parameters are the same as in Fig. 1.

teraction Hamiltonian in the basis of \hat{D} and \hat{B} can be rewritten as [60]

$$\hat{H}'_{\text{EIT}} = \sqrt{Ng_-^2 + \Omega_c^2} (\hat{S}_{31} \hat{B} + \hat{S}_{13} \hat{B}^+). \quad (5)$$

Figure 1(d) shows the transmission spectrum for the σ_- -cavity mode \hat{a}_- , the BP mode \hat{B} , and the DSP mode \hat{D} . The cavity transmission spectrum includes three peaks: the strong central peak coincides well with the line of the DSP, while two small side peaks are in excellent agreement with the line of the BP. It can be further understood from Eq. (5) that the BP mode \hat{B} couples to the collective states \hat{S}_{31} with the coupling strength $\sqrt{Ng_-^2 + \Omega_c^2}$ and thus splits into two normal modes at frequencies $E_{\pm} = \omega_a \pm \sqrt{Ng_-^2 + \Omega_c^2}$ when $\Delta_a = \Delta_c = 0$ [70]. Due to the spontaneous emission of the excited state $|3\rangle$, the two peaks of splitting BP modes are relatively small, as shown in Fig. 1(d) (blue dashed line). However, in the absence of \hat{D} in \hat{H}'_{EIT} , we can see that the DSP is totally decoupled from the excited state and immune to the spontaneous emission, which leads to a high transmission in the middle peak shown in Fig. 1(d) (orange dotted line). Comparing Fig. 1(b) with Fig. 1(d), we notice that the nonreciprocal cavity DSP is obtained only for the σ_- -polarized left-propagating input light. Due to the nonreciprocal DSP, a nonreciprocal window with high transmission appears near the cavity resonant frequency. In Fig. 2, the contrast ratio $\eta = |\frac{T_- - T_+}{T_- + T_+}|$ and the insertion loss $L = -10 \log_{10} T_-$ (dB) are plotted to demonstrate the performance of the nonreciprocity. The simulation result shows that the contrast ratio η is near unity with low insertion loss $L \leq 2$ (dB) in the region of $|\Delta_p| \leq 0.31\gamma_3$.

Next, we focus on the DSP and quantitatively investigate the decay rate and the linewidth of the DSP. Under the condition of $\sqrt{Ng_-^2 + \Omega_c^2} \gg \kappa, \gamma_2, \gamma_3$ [70], the BP is separated well from the DSP, and thus, we can ignore the component of BP mode \hat{B} near the cavity resonant frequency. Then the cavity mode $\hat{a}_- \approx \cos\theta \hat{D}$, and $\hat{S}_{12} \approx -\sin\theta \hat{D}$. We set $\Delta_a = \Delta_c = 0$. The equation of motion for the DSP mode \hat{D} and its

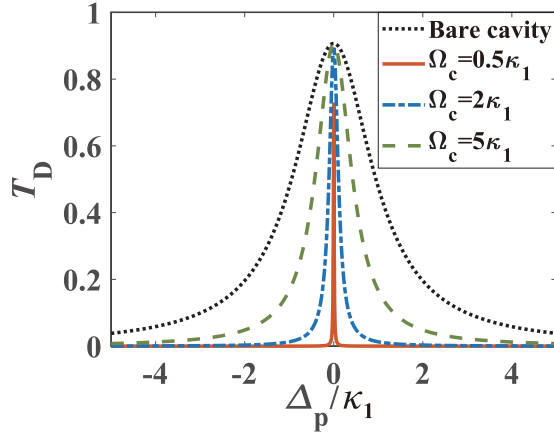


FIG. 3. Transmission T_D as a function of the normalized frequency detuning Δ_p/κ_1 for $\Omega_c = 0.5\kappa_1$, $\Omega_c = 2\kappa_1$, and $\Omega_c = 5\kappa_1$. The other parameters are the same as in Fig. 1.

steady-state solution are given by

$$\dot{\hat{D}} = -\left(i\Delta_p + \frac{\kappa_D}{2}\right)\hat{D} + \sqrt{\kappa_2} \cos\theta E_{p-}, \quad (6a)$$

$$\hat{D} = -\frac{\sqrt{\kappa_2} \cos\theta E_{p-}}{i\Delta_p + \frac{\kappa_D}{2}}, \quad (6b)$$

where $\kappa_D = \kappa \cos^2\theta + \gamma_2 \sin^2\theta$. From Eqs. (6a) and (6b), one can find that the decay rate of the DSP is determined by the decay rates κ and γ_2 , and the dark-state rotation angle is $\theta = \arctan \frac{\sqrt{N}g}{\Omega_c}$ [59,61,62]. In practice, γ_2 is several orders of magnitude smaller than κ and γ_3 . With decreasing Ω_c , the cavity linewidth narrows due to the small κ_D , as shown in Fig. 3. Thus, the lifetime of the cavity photons is enhanced by increasing the admixture of the long-lived atomic excitation in the DSP.

IV. NONRECIPROCAL QUANTUM STATISTICS

In addition to the transmission which reflects the mean photon number, there is growing interest in nonreciprocity of nonclassical features of the system [49–52]. In this part, the photon statistics that reveal the quantum nature of the transmitted light are investigated. We focus on the zero-time-delay second-order correlation function in the steady state, $g_{\pm}^{(2)}(0) = \text{Lim}_{t \rightarrow \infty} \frac{\langle \hat{a}(t)_{\pm}^{\dagger 2} \hat{a}(t)_{\pm}^2 \rangle}{\langle \hat{a}(t)_{\pm}^{\dagger} \hat{a}(t)_{\pm} \rangle^2}$. The conditions $g_{\pm}^{(2)}(0) > 1$ and $g_{\pm}^{(2)}(0) < 1$ characterize super-Poissonian and sub-Poissonian photon-number statistics [49–51].

According to the method described in [71–74], under weak excitation (truncating the Hilbert space at the two-quantum level), the wave function of the system for light incident from the left side of the cavity is approximately expressed as

$$|\psi(t)\rangle_+ = |0, 0\rangle + A_{10}|1, 0\rangle + \sum_k A_{0k}|0, 1\rangle + A_{20}|2, 0\rangle + \sum_k A_{1k}|1, 1\rangle + \sum_{k,l(k \neq l)} A_{0(k)}|0, 2\rangle, \quad (7)$$

where the state $|n, m\rangle$ represents n photons in the cavity and m atoms in the excited state [4]. The index k (l) of the coefficients' subscripts denotes the k th (l th) atom being excited. Then the approximate expression for the second-order correlation function in the steady state is given by

$$g_+^{(2)}(0) = \frac{2|A_{20}|^2}{(|A_{10}|^2 + N|A_{1k}|^2 + 2|A_{20}|^2)^2}. \quad (8)$$

When light is incident from the right side of the cavity, under the weak excitation, the wave function of the system is as follows:

$$\begin{aligned} |\psi(t)\rangle_- &= |0, 0, 0\rangle + A_{100}|1, 0, 0\rangle \\ &+ \sum_{k'} A_{0k'0}|0, 1, 0\rangle + \sum_{k'} A_{00}|0, 0, 1\rangle \\ &+ \sum_{k'} A_{1k'0}|1, 1, 0\rangle + \sum_{k'} A_{10k'}|1, 0, 1\rangle \\ &+ \sum_{k',l'(k' \neq l')} A_{0(k')}|0, 2, 0\rangle + \sum_{k',l'} A_{0k'l'}|0, 1, 1\rangle \\ &+ \sum_{k',l'(k' \neq l')} A_{00(k')}|0, 0, 2\rangle + A_{200}|2, 0, 0\rangle, \quad (9) \end{aligned}$$

where the state $|p, q, s\rangle$ implies there are p photons in the cavity, q atoms in the excited state [3], and s atoms in the excited state [2]. The index k' (l') of the coefficients' subscripts denotes the k' th (l' th) atom is in the excited state [3] or [2]. Then the second-order correlation function in the steady state is as follows:

$$g_-^{(2)}(0) = \frac{2|A_{200}|^2}{(|A_{100}|^2 + N|A_{1k'0}|^2 + N|A_{10k'}|^2 + 2|A_{200}|^2)^2}. \quad (10)$$

Further, the steady-state analytical solutions of coefficients in Eqs. (8) and (10) can be calculated using Schrödinger's equation (see Appendix B). Here, we stress that the coefficient A_{10} (A_{100}) corresponds to the one-photon excitation, while the coefficient A_{20} (A_{200}) is related to the two-photon excitation. Due to the weak driving field, we have $|A_{10}| \gg |A_{20}|$, $|A_{1k}|$ ($|A_{100}| \gg |A_{200}|$, $|A_{1k'0}|$, $|A_{10k'}|$). Thus, the mean photon number in the cavity $\langle \hat{a}_+^{\dagger} \hat{a}_+ \rangle$ ($\langle \hat{a}_-^{\dagger} \hat{a}_- \rangle$) is almost equal to $|A_{10}|^2$ ($|A_{100}|^2$), and the transmission related to the one-photon excitation can be indicated as $|A_{10}/E_{p+}|^2$ ($|A_{100}/E_{p-}|^2$). For simplicity, we define the strength of driving fields as $E_{p+} = E_{p-} \equiv E$, and the transmission can be reduced as $|A_{10}/E|^2$ ($|A_{100}/E|^2$).

To demonstrate the nonreciprocity of photon statistics intuitively, the variation of $\log_{10}[g_{\pm}^{(2)}(0)]$ (red dot-dashed line) is plotted as a function of the probe detuning Δ_p/κ_1 under the two-photon resonance ($\Delta_a - \Delta_c = 0$) and nonresonance ($\Delta_a - \Delta_c \neq 0$) conditions in the single-atom ($N = 1$) and multiatom (for $N = 5$ as an example) cases. For convenience, we set $\Delta_c = 0$ throughout the paper. We also plot the transmission $|A_{10}/E|^2$ ($|A_{100}/E|^2$) (blue solid line) to analyze the photon statistics and the transmission properties at the same time. Comparing Figs. 4(a1), 4(a3), 4(b1),

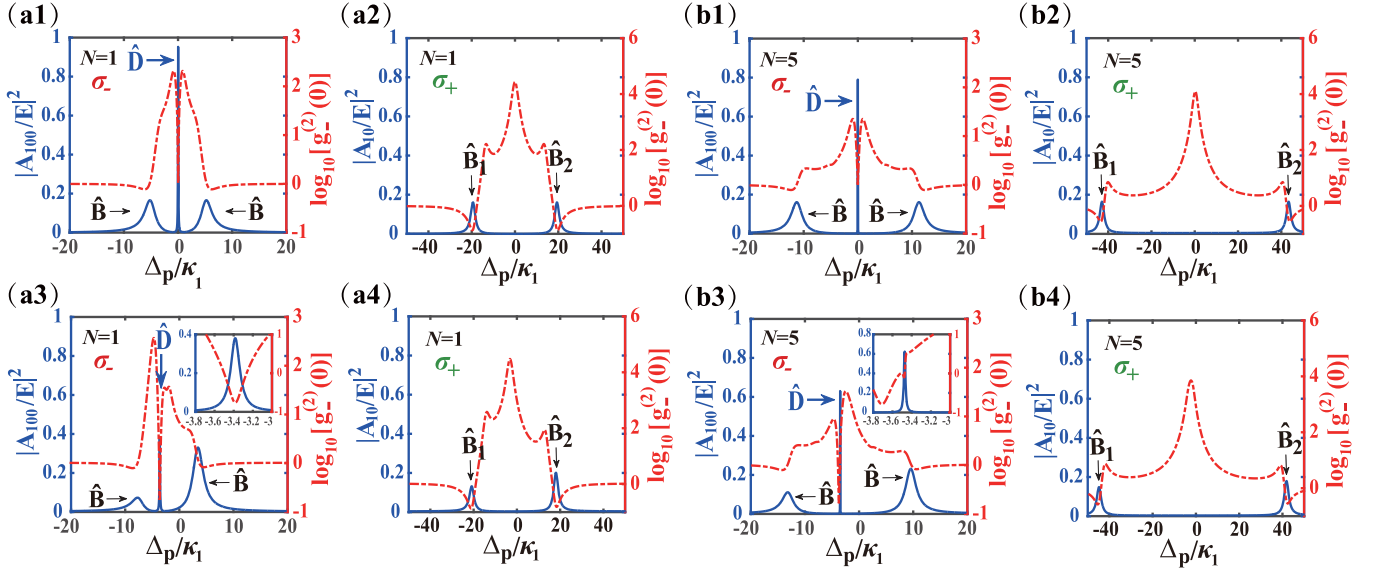


FIG. 4. Transmission spectrum $|A_{100}/E|^2/|A_{10}/E|^2$ corresponding to one-photon excitation (blue solid line) and nonreciprocal quantum statistics indicated by $\log_{10}[g_-^{(2)}(0)]/\log_{10}[g_+^{(2)}(0)]$ (red dot-dashed line). (a1)–(a4) $N = 1$ and (b1)–(b4) $N = 5$. (a1) and (b1) $\Omega_c = \kappa_1$, $\Delta_a = 0$; (a2) and (b2) $\Omega_c = 0$, $\Delta_a = 0$; (a3) and (b3) $\Omega_c = \kappa_1$, $\Delta_a = 3.5\kappa_1$; and (a4) and (b4) $\Omega_c = 0$, $\Delta_a = 3.5\kappa_1$. $E_{p+} = E_{p-} \equiv E$, $E = 0.01\kappa_1$, $\gamma_3 = 1.5\kappa_1$, $g_- = 5\kappa_1$, $g_+ = \sqrt{15}g_-$, and $\Delta_c = 0$. The other parameters are the same as in Fig. 1. The actual parameters can be referred to [75,76]

and 4(b3) with Figs. 4(a2), 4(a4), 4(b2), and 4(b4), we can see that the photon statistical properties are significantly different for the left-propagating σ_- and right-propagating σ_+ transmitted light. Such nonreciprocal quantum statistics is due to the existence of the nonreciprocal cavity DSP. In the following, we focus on the DSP frequency region. From Figs. 4(a1) and 4(b1) for single-atom and multiatom cases under the two-photon resonance condition, it can be seen that $g_-^{(2)}(0)$ tends to be unity ($\log_{10}[g_-^{(2)}(0)] \approx 0$) at the DSP point ($\Delta_p = 0$), which indicates that the left-propagating σ_- photons behave nearly like the feature of a coherent field in spite of having very high transmission ($|A_{100}/E|^2 \approx 1$). Such behavior can also be deduced from the analytical solutions in Eqs. (B18)–(B20) (see Appendix B). When the intracavity two-photon resonance condition of $\Delta_a - \Delta_c = 0$ is met, the DSP appears at the frequency point $\Delta_p = 0$, and the term $\Omega_c^2/D_2 \gg 1$. Then we have $T_1 \rightarrow 0$, $A_{100} \simeq -i\sqrt{\kappa_2}E_{p-}/K$, and $A_{200} \simeq -i\sqrt{2\kappa_2}E_{p-}A_{100}/(2K)$. Thus, we can obtain $g_-^{(2)}(0) \simeq 2|A_{200}|^2/|A_{100}|^4 \rightarrow 1$. In comparison, the right-propagating σ_+ photons have a super-Poissonian effect ($\log_{10}[g_+^{(2)}(0)] > 4$) with almost vanishing cavity occupation ($|A_{100}/E|^2 \approx 0$), as shown in Figs. 4(a2) and 4(b2). In order to realize the cavity DSP with nonclassical statistics, we tune the two-photon detuning $\Delta_a - \Delta_c$ off resonance and find that the DSP is obtained under the proper parameters in Fig. 4(a3) for the single-atom ($N = 1$) system, which has an apparent sub-Poissonian distribution ($\log_{10}[g_-^{(2)}(0)] \approx -0.76$) and simultaneously has a relatively high transmission ($|A_{100}/E|^2 \approx 40\%$) as well as a narrow bandwidth. During the investigation, we also find that the apparent sub-Poissonian distribution of the DSP cannot exist in multiatom systems, as shown in Fig. 4(b3) with $N = 5$ as an example ($\log_{10}[g_-^{(2)}(0)] \approx -0.1$). In contrast, the statistics of

the right-propagating σ_+ photons remain super-Poissonian ($\log_{10}[g_+^{(2)}(0)] > 3$), as shown in Figs. 4(a4) and 4(b4). Finally, the nonreciprocal cavity DSP is realized simultaneously with pronounced sub-Poissonian statistics, relatively high transmission, and a narrow bandwidth. It is worth noting that the excited state $|3\rangle$ is induced by the dark state $|\hat{D}\rangle$ due to the nonzero two-photon detuning, which accounts for the loss of the transmission of the DSP. Similar to the principle of unconventional photon statistics [77], such sub-Poissonian behavior of the DSP arises from the quantum interference between different excitation paths.

In order to gain deeper physical insight into the above results, we demonstrate the three processes contributing to the transmission of two photons and give a brief coupling schematic in Figs. 5(a) and 5(b), respectively. Process 1 in Fig. 5(a) represents two photons from the driving field E passing through the cavity without being absorbed, which corresponds to the path $|0, 0, 0\rangle \xrightarrow{i\sqrt{\kappa_2}E} |1, 0, 0\rangle \xrightarrow{i\sqrt{2\kappa_2}E} |2, 0, 0\rangle$ seen in Fig. 5(b). Process 2 in Fig. 5(a) indicates the two transmitted photons consist of the transmission of one unabsorbed photon and one photon emitted by an excited atom, which is related to the path $|0, 0, 0\rangle \xrightarrow{i\sqrt{\kappa_2}E} |1, 0, 0\rangle \xrightarrow{g_-} |0, 1, 0\rangle \xrightarrow{i\sqrt{\kappa_2}E} |1, 1, 0\rangle \xrightarrow{\sqrt{2}g_-} |2, 0, 0\rangle$ in Fig. 5(b). Process 3 in Fig. 5(a) shows one of the two transmitted photons is emitted from the excited atom and the other is directly emitted from the photon of the driving field without being absorbed, which corresponds to the path $|0, 0, 0\rangle \xrightarrow{i\sqrt{\kappa_2}E} |1, 0, 0\rangle \xrightarrow{g_-} |0, 1, 0\rangle \xrightarrow{\Omega_c} |0, 0, 1\rangle \xrightarrow{i\sqrt{\kappa_2}E} |1, 0, 1\rangle \xrightarrow{\Omega_c} |1, 1, 0\rangle \xrightarrow{\sqrt{2}g_-} |2, 0, 0\rangle$ in Fig. 5(b). When the two-photon resonance condition is met ($\Delta_a - \Delta_c = 0$), the DSP appears at the frequency point $\Delta_p = 0$. As mentioned

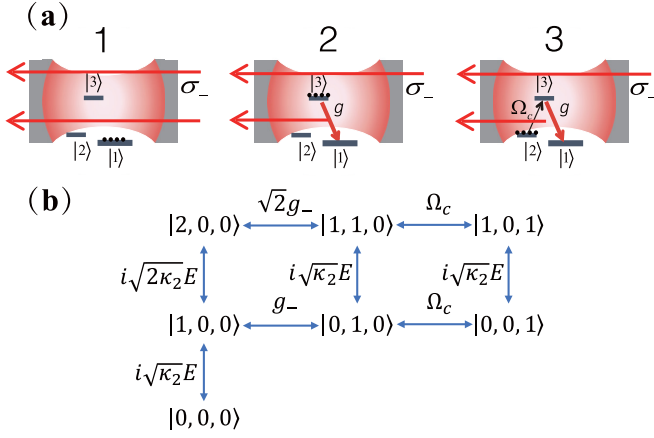


FIG. 5. (a) Diagrammatic representation of the processes (labeled 1, 2, and 3) which contribute to the two-photon transmission. (b) The coupling schematic corresponding to the relative transitions.

above, we set $\Delta_c = 0$ throughout the paper for convenience. Due to the almost completely destructive quantum interference, the probabilities $|A_{010}|^2$ and $|A_{110}|^2$ are extremely small [red dash-dotted lines in Figs. 6(a) and 6(b)], while $|A_{001}|^2$ and $|A_{101}|^2$ are relatively large under the control of Ω_c [yellow dotted lines in Figs. 6(a) and 6(b)]. Thus, it can be deduced that the excitation path associated with process 2 is nearly blocked and, at the same time, the apparent sub-Poissonian statistics of the DSP cannot exist for $A_{100} \simeq -i\sqrt{\kappa_2}E_p-/K$ and $A_{200} \simeq -i\sqrt{2\kappa_2}E_p \cdot A_{100}/(2K)$, which are almost independent of the parameters Ω_c and g_- . Once the two-photon resonance condition is broken (i.e., $\Delta_a \neq 0$), the states $|0, 1, 0\rangle$ and $|1, 1, 0\rangle$ have a non-negligible population, as shown in

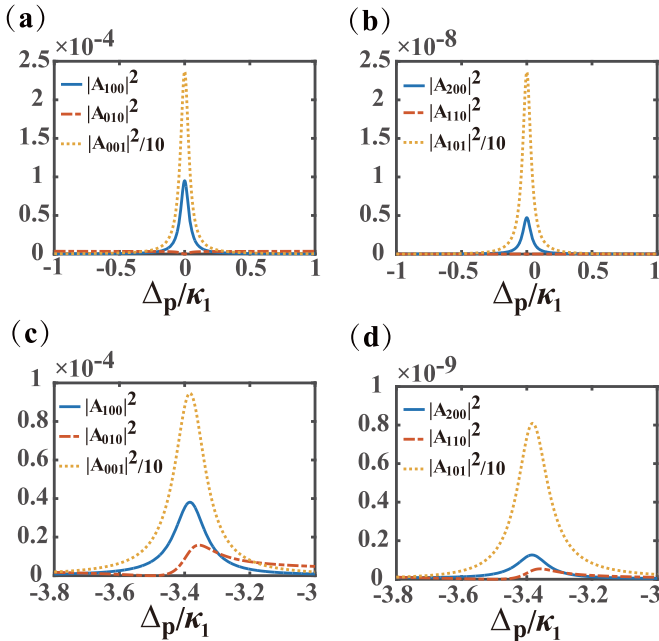


FIG. 6. The probabilities (a) and (c) $|A_{100}|^2$, $|A_{010}|^2$, and $|A_{001}|^2/10$ and (b) and (d) $|A_{200}|^2$, $|A_{110}|^2$, and $|A_{101}|^2/10$ versus the normalized detuning Δ_p/κ_1 . $\Delta_a = 0$ in (a) and (b), and $\Delta_a = 3.5\kappa_1$ in (c) and (d). The other parameters are the same as in Fig. 4(a3).

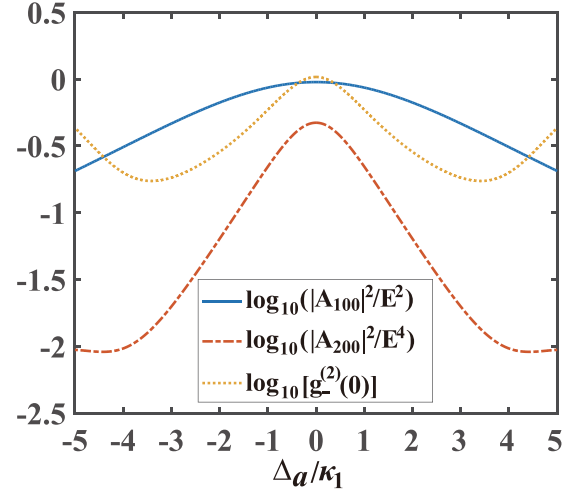


FIG. 7. The logarithms of $|A_{100}|^2/E^2$, $|A_{200}|^2/E^4$, and $g_-^{(2)}(0)$ versus the normalized detuning Δ_a/κ_1 . Δ_p is taken at the peak of DSP. The other parameters are the same as in Fig. 4(a3).

Figs. 6(c) and 6(d), due to the incompletely destructive interference, and the path corresponding to process 2 contributes to the quantum interference. Figure 7 shows that $|A_{100}|^2$ starts to decrease as $|\Delta_a|$ increases, while $|A_{200}|^2$ decreases quickly first and then increases slightly. Because the decrease rate of $|A_{200}|^2$ is faster than that of $|A_{100}|^2$, we can finally get a small value of $|A_{200}|^2$ and a relatively large value of $|A_{100}|^2$ at the same time with the proper parameters. Thus, a DSP with pronounced sub-Poissonian distribution statistics can be obtained with relatively high one-photon transmission as well as a narrow bandwidth, which represents the long lifetime of cavity photons. Meanwhile, the parameters Ω_c and g_- participate in the quantum interference between different paths.

Further, we investigate the effects of the parameters Δ_c , Δ_a , g_- , and Ω_c on the photon statistics of the left-propagating σ_- -polarized light in the single-atom case. In the following, we focus only on the DSP frequency region in which the photon statistics of the DSP have the sub-Poissonian property for $\log_{10}[g_{\pm}^{(2)}(0)] \leq -0.3$ and a relatively high transmission for $|A_{100}/E|^2 \geq 0.3$. In order to visualize the positions of DSP peaks under different parameters, we plot the variation of $|A_{100}/E|^2$ on the Δ_p - Δ_c plane and Δ_p - g_- plane. In Figs. 8(a1) and 8(a2), the peaks of the DSP are labeled 1, 2, and 3 for different values of Δ_a and Ω_c . Figures 8(b1) and 8(b2) show the variation of $-\log_{10}[g_-^{(2)}(0)]$ in the Δ_p - Δ_c plane and Δ_p - g_- plane for different values of Δ_a and Ω_c , respectively. According to Fig. 8(b1), with increasing Δ_a ($\Delta_a = 2\kappa_1, 3\kappa_1, 4\kappa_1$), region 1 transforms to regions 2 and 3 in turn. As a result, the nonclassical statistical region can be controlled; that is, the sub-Poissonian and super-Poissonian features of the DSP can be switched by tuning the parameters Δ_a and Δ_c . In Fig. 8(b2), the sub-Poissonian effect can be further enhanced by increasing the coupling strength g_- . By manipulating the strength of the control field Ω_c ($\Omega_c = \kappa_1, 2\kappa_1, 3.5\kappa_1$), the areas satisfying the conditions $\log_{10}[g_{\pm}^{(2)}(0)] \leq -0.3$ and $|A_{100}/E|^2 \geq 0.3$ appear in regions 1, 2, and 3. According to the above analysis, the statistical properties of the DSP can be manipulated by the external parameters Δ_c and Ω_c and

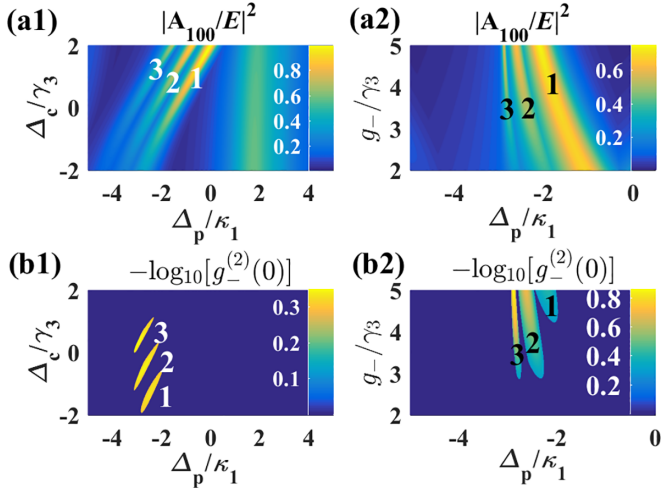


FIG. 8. The variation of (a1) and (a2) transmission $|A_{100}/E|^2$ and (b1) and (b2) the correlation function $g_-^{(2)}(0)$ on the Δ_p - Δ_c and Δ_p - g_- planes. (a1) and (b1) $\Omega_c = \kappa_1$ and $\Delta_a = 2\kappa_1$ (region 1), $3\kappa_1$ (region 2), and $4\kappa_1$ (region 3); (a2) and (b2) $\Omega_c = \kappa_1$ (region 1), $2\kappa_1$ (region 2), and $3.5\kappa_1$ (region 3) and $\Delta_a = 3.5\kappa_1$. The other parameters are the same as in Fig. 4(a3).

the system parameters Δ_a and g_- . Further, a nonreciprocal DSP can be obtained with simultaneous nonclassical statistics, relatively high transmission, and long photon lifetime with the proper choice of parameters.

V. EXPERIMENTAL FEASIBILITY

We briefly discuss the experimental feasibility of the proposed scheme. Here, we consider ^{85}Rb atoms as an example to show feasible coupling schemes. The hyperfine Zeeman

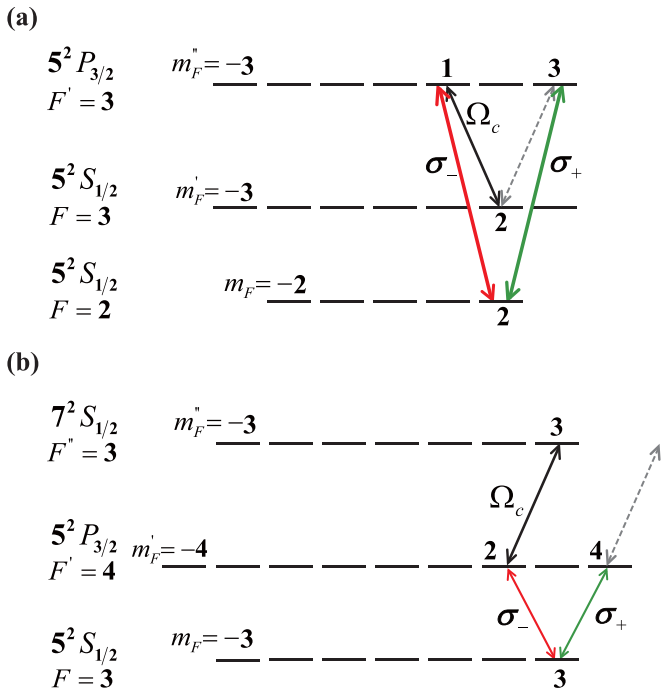


FIG. 9. Illustration of two examples of the feasible coupling schemes using ^{85}Rb atoms.

states $|5^2S_{1/2}, F = 2, m_F = 2\rangle$ and $|5^2S_{1/2}, F = 3, m_F = 2\rangle$ can be selected as the two ground states |1) and |2), with $|5^2P_{3/2}, F = 3, m_F = 3\rangle$ and $|5^2P_{3/2}, F = 3, m_F = 1\rangle$ being the two degenerate excited states |3) and |4), as shown in Fig. 9(a). We can also choose the hyperfine Zeeman states $|5^2S_{1/2}, F = 3, m_F = 3\rangle$ and $|7^2S_{1/2}, F = 3, m_F = 3\rangle$ as the two ground states |1) and |2) and $|5^2P_{3/2}, F = 4, m_F = 2\rangle$ and $|5^2P_{3/2}, F = 4, m_F = 4\rangle$ as the two degenerate excited states |3) and |4), as shown in Fig. 9(b). Furthermore, the nonreciprocal DSP can also be reversed by initially preparing the ^{85}Rb atoms in the states $|5^2S_{1/2}, F = 2, m_F = -2\rangle$ in Fig. 9(a) and $|5^2S_{1/2}, F = 3, m_F = -3\rangle$ in Fig. 9(b). The polarization-momentum locking of the input light can be realized by external apparatuses [46–48,58]. The feasible parameters in Sec. IV can be taken as $(g_+, \kappa, \gamma_3)/2\pi = (14, 0.66, 3)$ MHz [76] or $(g_+, \kappa, \gamma_3)/2\pi = (20, 2, 3)$ MHz [75].

VI. CONCLUSION

In summary, we proposed a nonreciprocal DSP by using an intracavity EIT with spin-biased cold atoms. The DSP can be accessed only from a given direction. For the DSP on resonance, due to the inhibition of the spontaneous emission, a high-performance nonreciprocal window with a near-unity contrast ratio and low insertion loss was created. The decay rate and the linewidth of the DSP were investigated. It was found that the decay rate is dominantly determined by the cavity decay rate and the dark-state angle. By increasing the admixture of the atomic excitation in the DSP, the linewidth is narrowed, which indicates the enhanced lifetime of the cavity photons in the form of the DSP. Next, we studied the photon statistics for light from both directions in the single-atom and multiatom cases. Due to the nonreciprocal DSP, the statistics is also nonreciprocal. By selecting the proper parameters in the single-atom case, a DSP with an apparent sub-Poissonian distribution was obtained which still possesses relatively high transmission and a narrow bandwidth. The nonreciprocal DSP proposed in this paper may provide the potential for novel quantum nonreciprocal devices and platforms in quantum simulations [53–57].

ACKNOWLEDGMENTS

This work was supported by the Shandong Natural Science Foundation, China (Grant No. ZR2021LLZ006); the National Natural Science Foundation of China (NSFC; Grants No. 61675118 and 61773245); the National Key Research and Development Program of China (Grant No. 2017YFA0701003); the Taishan Scholars Program of Shandong Province, China (Grant No. ts20190936); and the Shandong Provincial Natural Science Foundation (Grant No. ZR2021MA081).

APPENDIX A: DERIVATION OF OPERATORS IN SECTION III

For the right-propagating input light, the evolution equations of the relevant operators derived from the Langevin

equations are as follows:

$$\dot{\hat{a}}_+ = - \left(i\Delta_p + \frac{\kappa}{2} \right) \hat{a}_+ - ig_+ \sum_{j=1}^N \hat{\sigma}_{14}^{(j)} + \sqrt{\kappa_1} E_{p_+}, \quad (\text{A1})$$

$$\dot{\hat{\sigma}}_{14}^{(j)} = -i(\Delta_a + \Delta_p - i\gamma_4) \hat{\sigma}_{14}^{(j)} + ig_+ \hat{a}_+ (\hat{\sigma}_{44}^{(j)} - \hat{\sigma}_{11}^{(j)}). \quad (\text{A2})$$

By using the Langevin equations, the evolution equations of the relevant operators for the left-propagating input light are given by

$$\dot{\hat{a}}_- = - \left(i\Delta_p + \frac{\kappa}{2} \right) \hat{a}_- - ig_- \sum_{j=1}^N \hat{\sigma}_{13}^{(j)} + \sqrt{\kappa_2} E_{p_-}, \quad (\text{A3})$$

$$\begin{aligned} \dot{\hat{\sigma}}_{13}^{(j)} = & -i(\Delta_a + \Delta_p - i\gamma_3) \hat{\sigma}_{13}^{(j)} - i\Omega_c \hat{\sigma}_{12}^{(j)} \\ & + ig_- \hat{a}_- (\hat{\sigma}_{33}^{(j)} - \hat{\sigma}_{11}^{(j)}), \end{aligned} \quad (\text{A4})$$

$$\begin{aligned} \dot{\hat{\sigma}}_{12}^{(j)} = & -i(\Delta_a + \Delta_p - \Delta_c - i\gamma_2) \hat{\sigma}_{12}^{(j)} - i\Omega_c \hat{\sigma}_{13}^{(j)} \\ & + ig_- \hat{a}_- \hat{\sigma}_{32}^{(j)}. \end{aligned} \quad (\text{A5})$$

In the weak-field approximation, the steady-state solutions of the cavity modes \hat{a}_+ and $\hat{\sigma}_{14}^{(j)}$ for the right-propagating input light and \hat{a}_- and $\hat{\sigma}_{12}^{(j)}$ for the left-propagating input light can be derived, respectively, as

$$\hat{a}_+ = \frac{\sqrt{\kappa_1} E_{p_+}}{i\Delta_p + \frac{\kappa}{2} + \frac{Ng_+^2}{i(\Delta_a + \Delta_p) + \gamma_4}}, \quad (\text{A6})$$

$$\hat{\sigma}_{14}^{(j)} = - \frac{g_+ \hat{a}_+}{\Delta_a + \Delta_p - i\gamma_4}, \quad (\text{A7})$$

$$\hat{a}_- = \frac{\sqrt{\kappa_2} E_{p_-}}{i\Delta_p + \frac{\kappa}{2} + \frac{Ng_-^2}{i(\Delta_a + \Delta_p) + \gamma_3 + \frac{\Omega_c^2}{i(\Delta_a + \Delta_p - \Delta_c) + \gamma_2}}}, \quad (\text{A8})$$

$$\hat{\sigma}_{12}^{(j)} = \frac{\Omega_c g_- \hat{a}_-}{(\Delta_a + \Delta_p - i\gamma_3)(\Delta_a + \Delta_p - \Delta_c - i\gamma_2) - \Omega_c^2}. \quad (\text{A9})$$

APPENDIX B: DERIVATION OF PROBABILITY AMPLITUDES IN SECTION IV

For light input from the left side of the cavity, we obtain a set of the evolution equations for the coefficients using Schrödinger's equation $i\hbar|\dot{\psi}(t)\rangle_+ = \hat{H}'|\psi(t)\rangle_+$:

$$\dot{A}_{10} = - \frac{i}{\hbar} \left\{ KA_{10} + \sum_{i=1}^N g_+^{(i)} A_{0i} + i\sqrt{\kappa_1} E_{p_+} \right\}, \quad (\text{B1})$$

$$\dot{A}_{0k} = - \frac{i}{\hbar} \{ D_4 A_{0k} + g_+^{(k)} A_{10} \}, \quad (\text{B2})$$

$$\dot{A}_{20} = - \frac{i}{\hbar} \left\{ 2KA_{20} + \sqrt{2} \sum_{i=1}^N g_+^{(i)} A_{1i} + i\sqrt{2\kappa_1} E_{p_+} A_{10} \right\}, \quad (\text{B3})$$

$$\begin{aligned} \dot{A}_{1k} = & - \frac{i}{\hbar} \left\{ [K + D_{14}] A_{1k} + \sum_{l=1}^N g_+^{(l)} A_{0(l)} \right. \\ & \left. + i\sqrt{\kappa_1} E_{p_+} A_{0k} + \sqrt{2} g_+^{(k)} A_{20} \right\}, \end{aligned} \quad (\text{B4})$$

$$\dot{A}_{0(k)} = - \frac{i}{\hbar} \{ 2D_4 A_{0(k)} + g_+^{(k)} A_{11} + g_+^{(l)} A_{1k} \}, \quad (\text{B5})$$

where we take $K = \Delta_p - i\frac{\kappa}{2}$ and $D_4 = \Delta_a + \Delta_p - i\gamma_4$. In the steady state, by setting the time derivatives equal to zero, the solutions of the above equations are as follows:

$$A_{10} = - \frac{i\sqrt{\kappa_1} E_{p_+}}{K - \frac{Ng_+^2}{D_4}}, \quad A_{0k} = \frac{i\sqrt{\kappa_1} E_{p_+} g_+}{KD_4 - Ng_+^2}, \quad (\text{B6})$$

$$\begin{aligned} A_{20} = & - \frac{i\sqrt{2\kappa_1} E_{p_+}}{2K - 2Ng_+^2/D} A_{10} \\ & + \frac{i\sqrt{\kappa_1} E_{p_+}}{2K - 2Ng_+^2/D} \frac{\sqrt{2}Ng_+}{D} A_{0k}, \end{aligned} \quad (\text{B7})$$

$$A_{1k} = - \frac{i\sqrt{\kappa_1} E_{p_+}}{D} A_{0k} + \frac{\sqrt{2}g_+}{D} A_{20}, \quad (\text{B8})$$

where $D = K + D_4 - \frac{(N-1)g_+^2}{D_4}$ and we set $g_+^{(j)} \equiv g_+$ ($j = 1, 2, \dots, N$). When light is incident from the right side of the cavity, using Schrödinger's equation $i\hbar|\dot{\psi}(t)\rangle_- = \hat{H}'|\psi(t)\rangle_-$, the set of evolution equations for the coefficients is given by

$$\dot{A}_{100} = - \frac{i}{\hbar} \left\{ KA_{100} + \sum_{k'=1}^N A_{0k'0} g_-^{(k')} + i\sqrt{\kappa_2} E_{p_-} \right\}, \quad (\text{B9})$$

$$\dot{A}_{0k'0} = - \frac{i}{\hbar} \{ D_3 A_{0k'0} + \Omega_c A_{00k'} + g_-^{(k')} A_{100} \}, \quad (\text{B10})$$

$$\dot{A}_{00k'} = - \frac{i}{\hbar} \{ D_2 A_{00k'} + \Omega_c A_{0k'0} \}, \quad (\text{B11})$$

$$\begin{aligned} \dot{A}_{1k'0} = & - \frac{i}{\hbar} \left\{ (K + D_3) A_{1k'0} + \Omega_c A_{10k'} + \sqrt{2} g_-^{(k')} A_{200} \right. \\ & \left. + \sum_{l'=1}^N g_-^{(l')} A_{0(l')0} + i\sqrt{\kappa_2} E_{p_-} A_{0k'0} \right\}, \end{aligned} \quad (\text{B12})$$

$$\begin{aligned} \dot{A}_{10k'} = & - \frac{i}{\hbar} \left\{ (K + D_2) A_{10k'} + \sum_{l'=1}^N g_-^{(l')} A_{0l'k'} \right. \\ & \left. + \Omega_c A_{1k'0} + i\sqrt{\kappa_2} E_{p_-} A_{00k'} \right\}, \end{aligned} \quad (\text{B13})$$

$$\begin{aligned} \dot{A}_{0(l')0} = & - \frac{i}{\hbar} \left\{ 2D_3 A_{0(l')0} + g_-^{(l')} A_{1k'0} + g_-^{(k')} A_{1l'0} \right. \\ & \left. + \Omega_c (A_{0k'l'} + A_{0l'k'}) \right\}, \end{aligned} \quad (\text{B14})$$

$$\begin{aligned} \dot{A}_{0k'l'} = & - \frac{i}{\hbar} \left\{ (D_3 + D_2) A_{0k'l'} + \Omega_c (A_{00(k')} + A_{0(l')0}) \right. \\ & \left. + g_-^{(k')} A_{10l'} \right\}, \end{aligned} \quad (\text{B15})$$

$$\dot{A}_{00(l')} = - \frac{i}{\hbar} \left\{ 2D_2 A_{00(l')} + \Omega_c (A_{0k'l'} + A_{0l'k'}) \right\}, \quad (\text{B16})$$

$$\begin{aligned} \dot{A}_{200} = & - \frac{i}{\hbar} \left\{ 2KA_{200} + \sqrt{2} \sum_{k'=1}^N g_-^{(k')} A_{1k'0} \right. \\ & \left. + i\sqrt{2\kappa_2} E_{p_-} A_{100} \right\}. \end{aligned} \quad (\text{B17})$$

Here, we define $D_3 = \Delta_a + \Delta_p - i\gamma_3$ and $D_2 = \Delta_a + \Delta_p - \Delta_c - i\gamma_2$. In the steady state, the analytical solutions of the coefficients are presented as

$$A_{100} = -\frac{i\sqrt{\kappa_2}E_{p-}}{K - \frac{Ng_-^2}{D_3 - \Omega_c^2/D_2}}, \quad (\text{B18})$$

$$A_{0k'0} = -\frac{g_-}{D_3 - \Omega_c^2/D_2}A_{100}, \quad A_{00k'} = -\frac{\Omega_c}{D_2}A_{0k'0}, \quad (\text{B19})$$

$$A_{200} = -\frac{i\sqrt{2\kappa_2}E_{p-}}{2K - N(\sqrt{2}g_-)^2T_3}A_{100} + \frac{i\sqrt{\kappa_2}E_{p-}N\sqrt{2}g_-T_3}{2K - N(\sqrt{2}g_-)^2T_3}A_{0k'0} - \frac{N\sqrt{2}g_-T_3T_4}{2K - N(\sqrt{2}g_-)^2T_3}A_{00k'}, \quad (\text{B20})$$

$$A_{1k'0} = T_3T_4A_{00k'} - \sqrt{2}g_-T_3A_{200} - i\sqrt{\kappa_2}E_{p-}T_3A_{0k'0}, \quad (\text{B21})$$

$$A_{10k'} = -\frac{\Omega_c}{K + D_2}[1 + (N-1)g_-^2T_1T_2]A_{1k'0} - \frac{i\sqrt{\kappa_2}E_{p-}}{K + D_2}[1 + \frac{(N-1)g_-^2}{K + D_2}T_1]A_{00k'}, \quad (\text{B22})$$

where $T_1 = (D_2 + D_3 - \frac{\Omega_c^2}{D_2} - \frac{\Omega_c^2}{D_3} - \frac{(N-1)g_-^2}{K+D_2})^{-1}$, $T_2 = \frac{1}{D_3} + \frac{1}{K+D_2}$, $T_3 = [K + D_3 - \frac{\Omega_c^2}{K+D_2} - (N-1)g_-^2\Omega_c^2T_1T_2^2 - \frac{(N-1)g_-^2}{D_3}]^{-1}$, and $T_4 = \frac{i\sqrt{\kappa_2}E_{p-}\Omega_c}{K+D_2}[1 + (N-1)g_-^2T_1T_2]$.

-
- [1] C. Caloz, A. Alù, S. Tretyakov, D. Sounas, K. Achouri, and Z. L. Deck-Léger, Electromagnetic Nonreciprocity, *Phys. Rev. Appl.* **10**, 047001 (2018).
- [2] D. Jalas, A. Petrov, M. Eich, W. Freude, S. H. Fan, Z. F. Yu, R. Baets, M. Popović, A. Melloni, J. D. Joannopoulos, M. Vanwolleghem, C. R. Doerr, and H. Renner, What is—and what is not—an optical isolator, *Nat. Photonics* **7**, 579 (2013).
- [3] C. Gonzalez-Ballester, E. Moreno, F. J. Garcia-Vidal, and A. Gonzalez-Tudela, Nonreciprocal few-photon routing schemes based on chiral waveguide-emitter couplings, *Phys. Rev. A* **94**, 063817 (2016).
- [4] S. C. Zhang, G. W. Lin, and Y. Q. Hu, Cavity-Free Circulator with Low Insertion Loss Using Hot Atoms, *Phys. Rev. Appl.* **14**, 024032 (2020).
- [5] L. F. Liu, Y. Zhang, S. C. Zhang, J. Qian, S. Q. Gong, and Y. P. Niu, Magnetic-free unidirectional polarization rotation and free-space optical isolators and circulators, *Appl. Phys. Lett.* **121**, 261102 (2022).
- [6] S. Daiss, S. Langenfeld, S. Welte, E. Distant, P. Thomas, L. Hartung, O. Morin, and G. Rempe, A quantum-logic gate between distant quantum-network modules, *Science* **371**, 614 (2021).
- [7] J. I. Cirac, P. Zoller, H. J. Kimble, and H. Mabuchi, Quantum State Transfer and Entanglement Distribution among Distant Nodes in a Quantum Network, *Phys. Rev. Lett.* **78**, 3221 (1997).
- [8] H. J. Kimble, The quantum internet, *Nature (London)* **453**, 1023 (2008).
- [9] L. Fan, J. Wang, L. T. Varghese, H. Shen, B. Niu, Y. Xuan, A. M. Weiner, and M. H. Qi, An all-silicon passive optical diode, *Science* **335**, 447 (2012).
- [10] Y. Sun, Y. W. Tong, C. H. Xue, Y. Q. Ding, Y. H. Li, H. T. Jiang, and H. Chen, Electromagnetic diode based on nonlinear electromagnetically induced transparency in metamaterials, *Appl. Phys. Lett.* **103**, 091904 (2013).
- [11] L. Chang, X. S. Jiang, S. Y. Hua, C. Yang, J. M. Wen, L. Jiang, G. Y. Li, G. Z. Wang, and M. Xiao, Parity-time symmetry and variable optical isolation in active-passive-coupled microresonators, *Nat. Photonics* **8**, 524 (2014).
- [12] B. Peng, S. H. Kaya Özdemir, F. C. Lei, F. Monifi, M. Gianfreda, G. L. Long, S. H. Fan, F. Nori, C. M. Bender, and L. Yang, Parity-time-symmetric whispering-gallery microcavities, *Nat. Phys.* **10**, 394 (2014).
- [13] P. F. Yang, X. W. Xia, H. He, S. K. Li, X. Han, P. Zhang, G. Li, P. F. Zhang, J. P. Xu, Y. P. Yang, and T. C. Zhang, Realization of Nonlinear Optical Nonreciprocity on a Few-Photon Level Based on Atoms Strongly Coupled to an Asymmetric Cavity, *Phys. Rev. Lett.* **123**, 233604 (2019).
- [14] D. W. Wang, H. T. Zhou, M. J. Guo, J. X. Zhang, J. Evers, and S. Y. Zhu, Optical Diode Made from a Moving Photonic Crystal, *Phys. Rev. Lett.* **110**, 093901 (2013).
- [15] S. A. R. Horsley, J. H. Wu, M. Artoni, and G. C. La Rocca, Optical Nonreciprocity of Cold Atom Bragg Mirrors in Motion, *Phys. Rev. Lett.* **110**, 223602 (2013).
- [16] Z. F. Yu and S. H. Fan, Complete optical isolation created by indirect interband photonic transitions, *Nat. Photonics* **3**, 91 (2009).
- [17] M. S. Kang, A. Butsch, and P. St. J. Russell, Reconfigurable light-driven opto-acoustic isolators in photonic crystal fibre, *Nat. Photonics* **5**, 549 (2011).
- [18] K. J. Fang, Z. F. Yu, and S. H. Fan, Photonic Aharonov-Bohm Effect Based on Dynamic Modulation, *Phys. Rev. Lett.* **108**, 153901 (2012).
- [19] L. Q. Yuan, S. S. Xu, and S. H. Fan, Achieving nonreciprocal unidirectional single-photon quantum transport using the photonic Aharonov-Bohm effect, *Opt. Lett.* **40**, 5140 (2015).
- [20] M. Hafezi and P. Rabl, Optomechanically induced nonreciprocity in microring resonators, *Opt. Express* **20**, 7672 (2012).
- [21] X. W. Xu and Y. Li, Optical nonreciprocity and optomechanical circulator in three-mode optomechanical systems, *Phys. Rev. A* **91**, 053854 (2015).
- [22] Z. Shen, Y. L. Zhang, Y. Chen, C. L. Zou, Y. F. Xiao, X. B. Zou, F. W. Sun, G. C. Guo, and C. H. Dong, Experimental realization of optomechanically induced non-reciprocity, *Nat. Photonics* **10**, 657 (2016).

- [23] M. A. Miri, F. Ruesink, E. Verhagen, and A. Alù, Optical Nonreciprocity Based on Optomechanical Coupling, *Phys. Rev. Appl.* **7**, 064014 (2017).
- [24] N. R. Bernier, L. D. Tóth, A. Koottandavida, M. A. Loannou, D. Malz, A. Nunnenkamp, A. K. Feofanov, and T. J. Kippenberg, Nonreciprocal reconfigurable microwave optomechanical circuit, *Nat. Commun.* **8**, 604 (2017).
- [25] Z. Shen, Y. L. Zhang, Y. Chen, F. W. Sun, X. B. Zou, G. C. Guo, C. L. Zou, and C. H. Dong, Reconfigurable optomechanical circulator and directional amplifier, *Nat. Commun.* **9**, 1797 (2018).
- [26] X. W. Xu, L. N. Song, Q. Zheng, Z. H. Wang, and Y. Li, Optomechanically induced nonreciprocity in a three-mode optomechanical system, *Phys. Rev. A* **98**, 063845 (2018).
- [27] G. L. Li, X. Xiao, and Y. Li, Tunable optical nonreciprocity and a phonon-photon router in an optomechanical system with coupled mechanical and optical modes, *Phys. Rev. A* **97**, 023801 (2018).
- [28] F. Ruesink, J. P. Mathew, and M. A. Miri, Optical circulation in a multimode optomechanical resonator, *Nat. Commun.* **9**, 1798 (2018).
- [29] B. J. Li, R. Huang, and X. W. Xu, Nonreciprocal unconventional photon blockade in a spinning optomechanical system, *Photonics Res.* **7**, 630 (2019).
- [30] S. C. Zhang, Y. Q. Hu, G. W. Lin, Y. P. Niu, K. Y. Xia, J. B. Gong, and S. Q. Gong, Thermal-motion-induced non-reciprocal quantum optical system, *Nat. Photonics* **12**, 744 (2018).
- [31] S. C. Zhang, Y. F. Zhan, S. Q. Gong, and Y. P. Niu, Noiseless single-photon isolator at room temperature, *Commun. Phys.* **6**, 33 (2023).
- [32] K. Y. Xia, F. Nori, and M. Xiao, Cavity-Free Optical Isolators and Circulators Using a Chiral Cross-Kerr Nonlinearity, *Phys. Rev. Lett.* **121**, 203602 (2018).
- [33] G. W. Lin, S. C. Zhang, and Y. Q. Hu, Nonreciprocal Amplification with Four-Level Hot Atoms, *Phys. Rev. Lett.* **123**, 033902 (2019).
- [34] Y. Q. Hu, S. C. Zhang, and Y. H. Qi, Multiwavelength Magnetic-Free Optical Isolator by Optical Pumping in Warm Atoms, *Phys. Rev. Appl.* **12**, 054004 (2019).
- [35] C. Liang, B. Liu, A. N. Xu, X. Wen, C. C. Lu, K. Y. Xia, M. K. Tey, Y. C. Liu, and L. You, Collision-Induced Broadband Optical Nonreciprocity, *Phys. Rev. Lett.* **125**, 123901 (2020).
- [36] S. F. Fan, Y. H. Qi, G. W. Lin, Y. P. Niu, and S. Q. Gong, Broadband optical nonreciprocity in an N-type thermal atomic system, *Opt. Commun.* **462**, 125343 (2020).
- [37] M. X. Dong, K. Y. Xia, W. H. Zang, Y. C. Yu, Y. H. Ye, E. Z. Li, L. Zeng, D. S. Ding, B. S. Shi, G. C. Guo, and F. Nori, All-optical reversible single-photon isolation at room temperature, *Sci. Adv.* **7**, eabe8924 (2021).
- [38] F. Song, Z. P. Wang, E. Z. Li, B. L. Yu, and Z. X. Huang, Nonreciprocity with Structured Light Using Optical Pumping in Hot Atoms, *Phys. Rev. Appl.* **18**, 024027 (2022).
- [39] P. Lodahl, S. Mahmoodian, S. Stobbe, A. Rauschenbeutel, P. Schneeweiss, and J. Volz, Chiral quantum optics, *Nature (London)* **541**, 473 (2017).
- [40] C. Sayrin, C. Junge, R. Mitsch, B. Albrecht, and D. O'Shea, Nanophotonic Optical Isolator Controlled by the Internal State of Cold Atoms, *Phys. Rev. X* **5**, 041036 (2015).
- [41] M. Scheucher, A. Hilico, E. Will, J. Volz, and A. Rauschenbeutel, Quantum optical circulator controlled by a single chirally coupled atom, *Science* **354**, 1577 (2016).
- [42] K. Y. Xia, G. W. Lu, G. W. Lin, Y. Q. Cheng, Y. P. Niu, S. Q. Gong, and J. Twamley, Reversible nonmagnetic single-photon isolation using unbalanced quantum coupling, *Phys. Rev. A* **90**, 043802 (2014).
- [43] L. Tang, J. S. Tang, W. D. Zhang, G. W. Lu, H. Zhang, Y. Zhang, K. Y. Xia, and M. Xiao, On-chip chiral single-photon interface: Isolation and unidirectional emission, *Phys. Rev. A* **99**, 043833 (2019).
- [44] W. B. Yan, W. Y. Ni, J. Zhang, F. Y. Zhang, and H. Fan, Tunable single-photon diode by chiral quantum physics, *Phys. Rev. A* **98**, 043852 (2018).
- [45] Y. You, Y. Q. Hu, G. W. Lin, Y. H. Qi, Y. P. Niu, and S. Q. Gong, Quantum nonreciprocity based on electromagnetically induced transparency in chiral quantum-optical systems, *Phys. Rev. A* **103**, 063706 (2021).
- [46] M. X. Dong, Y. C. Yu, Y. H. Ye, W. H. Zhang, E. Li, L. Zeng, G. C. Guo, D. S. Ding, and B. S. Shi, Experimental realization of quantum non-reciprocity based on cold atomic ensembles, [arXiv:1908.09242](https://arxiv.org/abs/1908.09242).
- [47] L. Tang, J. S. Tang, and K. Y. Xia, Chiral quantum optics and optical nonreciprocity based on susceptibility-momentum locking, *Adv. Quantum Technol.* **5**, 2200014 (2022).
- [48] X. X. Hu, Z. B. Wang, P. F. Zhang, G. J. Chen, Y. L. Zhang, G. Li, X. B. Zou, T. C. Zhang, H. X. Tang, C. H. Dong, G. C. Guo, and C. L. Zou, Noiseless photonic non-reciprocity via optically-induced magnetization, *Nat. Commun.* **12**, 2389 (2021).
- [49] R. Huang, A. Miranowicz, J. Q. Liao, F. Nori, and H. Jing, Nonreciprocal Photon Blockade, *Phys. Rev. Lett.* **121**, 153601 (2018).
- [50] W. S. Xue, H. Z. Shen, and X. X. Yi, Nonreciprocal conventional photon blockade in driven dissipative atom-cavity, *Opt. Lett.* **45**, 4424 (2020).
- [51] X. W. Xia, X. Q. Zhang, J. P. Xu, H. Z. Li, Z. Y. Fu, and Y. P. Yang, Improvement of nonreciprocal unconventional photon blockade by two asymmetrical arranged atoms embedded in a cavity, *Opt. Express* **30**, 7907 (2022).
- [52] A. Graf, S. D. Rogers, J. Staffa, U. A. Javid, D. H. Griffith, and Q. Lin, Nonreciprocity in Photon Pair Correlations of Classically Reciprocal Systems, *Phys. Rev. Lett.* **128**, 213605 (2022).
- [53] *Quantum Simulations with Photons and Polaritons*, edited by D. G. Angelakis, Quantum Science and Technology (Springer, Cham, 2017).
- [54] M. J. Hartmann, F. G. S. L. Brandão, and M. B. Plenio, Strongly interacting polaritons in coupled arrays of cavities, *Nat. Phys.* **2**, 849 (2006).
- [55] C. Noh and D. G. Angelakis, Quantum simulations and many-body physics with light, *Rep. Prog. Phys.* **80**, 016401 (2017).
- [56] C. Noh and D. G. Angelakis, Simulating topological effects with photons in coupled QED cavity arrays, *Int. J. Mod. Phys. B* **28**, 1441003 (2014).
- [57] C. Lee, C. Noh, N. Schetakis, and D. G. Angelakis, Few-photon transport in many-body photonic systems: A scattering approach, *Phys. Rev. A* **92**, 063817 (2015).
- [58] P. F. Yang, M. Li, X. Han, H. He, G. Li, C.-L. Zou, P. F. Zhang, Y. H. Qian, and T. C. Zhang, Non-reciprocal cavity polariton

- with atoms strongly coupled to optical cavity, *Laser Photonics Rev.* **2200574** (2023).
- [59] M. Fleischhauer, A. Imamoglu, and J. P. Marangos, Electromagnetically induced transparency: Optics in coherent media, *Rev. Mod. Phys.* **77**, 633 (2005).
- [60] G. W. Lin, J. B. Gong, J. Yang, Y. H. Qi, X. M. Lin, Y. P. Niu, and S. Q. Gong, Optical cavity quantum electrodynamics with dark-state polaritons, *Phys. Rev. A* **89**, 043815 (2014).
- [61] J. Ningyuan, A. Georgakopoulos, A. Ryou, N. Schine, A. Sommer, and J. Simon, Observation and characterization of cavity Rydberg polaritons, *Phys. Rev. A* **93**, 041802(R) (2016).
- [62] M. D. Lukin, M. Fleischhauer, and M. O. Scully, Intracavity electromagnetically induced transparency, *Opt. Lett.* **23**, 295 (1998).
- [63] G. W. Lin, J. Yang, Y. P. Niu, and S. Q. Gong, Cavity linewidth narrowing with dark-state polaritons, *Chin. Phys. B* **25**, 014201 (2016).
- [64] M. Fleischhauer, S. F. Yelin, and M. D. Lukin, How to trap photons? Storing single-photon quantum states in collective atomic excitations, *Opt. Commun.* **179**, 395 (2000).
- [65] Y. You, G. W. Lin, L. J. Feng, Y. P. Niu, and S. Q. Gong, Quantum storage of single photons with unknown arrival time and pulse shapes, *Chin. Phys. B* **30**, 084207 (2021).
- [66] Y. F. Han, C. J. Zhu, X. S. Huang, and Y. P. Yang, Electromagnetic control and improvement of nonclassically in a strongly coupled single-atom cavity-QED system, *Phys. Rev. A* **98**, 033828 (2018).
- [67] G. W. Lin, Y. H. Qi, X. M. Lin, Y. P. Niu, and G. S. Qing, Strong photon blockade with intracavity electromagnetically induced transparency in a blockaded Rydberg ensemble, *Phys. Rev. A* **92**, 043842 (2015).
- [68] A. S. Manka, H. M. Doss, L. M. Narducci, and P. Ru, Spontaneous emission and absorption properties of a driven three-level system. II. The Λ and cascade models, *Phys. Rev. A* **43**, 3748 (1991).
- [69] D. F. Wall and G. J. Milburn, *Quantum Optics* (Springer, Berlin, 1994).
- [70] C. H. Dong, V. Fiore, M. Kuzyk, and H. Wang, Optomechanical dark mode, *Science* **338**, 1609 (2012).
- [71] G. Rempe, R. J. Thompson, and H. J. Kimble, Cavity quantum electrodynamics with strong coupling in the optical domain, *Phys. Scr.* **T51**, 67 (1994).
- [72] H. J. Carmichael, R. J. Brecha, and P. R. Rice, Quantum interference and collapse of the wavefunction in cavity QED, *Opt. Commun.* **82**, 73 (1991).
- [73] C. Noh, Interference-induced photon antibunching in a cavity QED setup with a three-level atom, *J. Korean Phys. Soc.* **77**, 60 (2020).
- [74] C. Noh, Emission of single photons in the weak coupling regime of the Jaynes Cummings model, *Sci. Rep.* **10**, 16076 (2020).
- [75] C. Hamsen, K. N. Tolazzi, T. Wilk, and G. Rempe, Two-Photon Blockade in an Atom-Driven Cavity QED System, *Phys. Rev. Lett.* **118**, 133604 (2017).
- [76] S. Gupta, K. L. Moore, K. W. Murch, and D. M. Stamper-Kurn, Cavity Nonlinear Optics at Low Photon Numbers from Collective Atomic Motion, *Phys. Rev. Lett.* **99**, 213601 (2007).
- [77] E. Zubizarreta Casalengua, J. C. López Carreño, F. P. Laussy, and E. del Valle, Conventional and unconventional photon statistics, *Laser Photonics Rev.* **14**, 1900279 (2020).